Journal of Optics
https://doi.org/10.1007/s12596-024-02136-x

RESEARCH ARTICLE

Comprehensive study of trivalent Dy^{3+} ions-incorporated zinc phosphate glasses for white light emission in solid-state photonic devices

S. Vidya Sagar[1] · K. Venkata Rao[1] · S. Babu[2] · SK. Annar[3]

Received: 27 October 2023 / Accepted: 5 August 2024

Abstract

In this study, the structural and optical properties of zinc phosphate (ZnP) glasses doped with different concentrations of Dy^{3+} ions in the composition (60-n)P_2O_5-20ZnO-10SrO-10LiF-nDy_2O_3 were investigated. Using the melt-quenching technique, these glasses were prepared and characterized by X-ray diffraction (XRD), scanning emission microscope (SEM), Fourier transform infrared (FTIR), Raman, absorption, and photoluminescence spectroscopy. SEM analysis and XRD profiles confirmed the amorphous nature of ZnP glasses. Furthermore, the presence of elements within its composition was validated via the employment of EDX. The FTIR spectra of the ZnP glasses exhibited vibration bands that were in line with the characteristic phosphate groups, which was further substantiated by Raman analysis. Judd-Ofelt (JO) theory was applied to calculate the intensity parameters Ω_t (t = 2,4,6), radiative transition probabilities (A_T), branching ratios (β), and radiative lifetimes (τ_{rad}) of Dy^{3+} ions. JO intensity parameter shows a trend $\Omega_6 > \Omega_2 > \Omega_4$. The emission spectra displayed three distinct bands, specifically the blue, yellow, and red bands, which corresponded to the transitions of the Dy^{3+} ions from the $^4F_{9/2}$ to the $^6H_{P/2}$ states (P = 15,13,11) upon being excited by a 350 nm wavelength. The Y/B intensity ratios that are higher than 1 (> 1) indicate a significant covalent character. The chromaticity colour coordinates (x_c, y_c), and correlated colour temperatures (CCT) of the glasses lie in the cool white light region. The results of this study suggest that ZnP glasses, when doped with Dy^{3+} ions, have the potential to serve as solid-state lighting materials capable of emitting white light.

Keywords Dy^{3+} doped glass · Zinc phosphate · JO Parameters · Photoluminescence (PL) · Chromaticity coordinates

Introduction

In recent times, glasses have become more commonplace in a variety of fields, such as photonics, displays, lasers, optical fibers, converters, and medicine [1, 2]. In recent decades, rare-earth activated glasses, especially oxide glasses, have attracted considerable attention because of their potential applications in various scientific and technological fields such as lighting, solar cells, photonics, and biomedicine [3, 4]. The extensive range of applications is a result of the versatile nature of optical f-f transitions that occur in lanthanide ions, leading to efficient luminescent bands that span across the entire visible spectrum [5]. Phosphate-based glasses exhibit low melting points, high refractive indices, and good transmittance in ultraviolet spectra in comparison to other oxide glasses [6–9]. Despite their attractive features, including their potential use in solid-state electrolytes [10], solid-state lasers [11], photonics, and biomedical materials [12], phosphate glasses have a few disadvantages, such as low mechanical strength, chemical resistance, and hygroscopicity [13]. However, this problem can be minimized by adding suitable network modifiers. Therefore, many researchers are interested in these glasses owing to their

✉ K. Venkata Rao
drvenkataraok@gmail.com

[1] Department of Physics, Government Degree College, Porumamilla, Kadapa, Andhra Pradesh 516193, India

[2] Department of Physics, Rajeev Gandhi Memorial College of Engineering & Technology, Nandyal, Andhra Pradesh 518501, India

[3] Department of Chemistry, DKW(A) Government Degree College, Nellore, Andhra Pradesh 524003, India

Published online: 22 August 2024

attractive properties. Rare-earth elements (REEs) -activated phosphate glasses possess distinctive and appealing spectral characteristics in the UV-Vis-NIR domains owing to the 4f–4f transitions [14]. 4f–4f transitions play a key role in utilization of these glasses in numerous applications, including luminescent materials and optical amplifiers [14].

Phosphate-based oxide glasses, renowned for their ability to serve as glass formers, have been merged with activator Dy^{3+} ions (REEs) in conjunction with the inclusion of network modifiers, including ZnO, SrO, and LiF, into the composition. In this work, Dy^{3+} was chosen as a rare-earth ion because it has many remarkable optical properties and applications in commercial photonic devices [15]. There are many advantages of using Dy^{3+} as a rare-earth ion for laser operation, colour display, and white light production [16]. The glass materials, activated by Dy^{3+} ions, have the capability to generate light within the visible spectrum and are accountable for the emission of blue light ($^4F_{9/2}\rightarrow{}^6H_{15/2}$) as well as yellow light ($^4F_{9/2}\rightarrow{}^6H_{15/2}$) [17]. Considering these emission transitions as well as the colour coordinates in the white region of the CIE1931 diagram, glasses that are doped/activated with Dy^{3+} ions with can be useful in the development of white light sources [18]. To mitigate several drawbacks associated with phosphate glasses, including diminished mechanical strength, chemical resistance, and hygroscopicity, network modifiers such as ZnO, SrO, and LiF have been incorporated [19]. Lithium fluoride (LiF) is added to the glass to maintain transparency [20]. The addition of fluorides to oxide glasses leads to a reduction in phonon energy and a resulting increase in luminescence intensity, both of which are crucial requirements for the development of white light emitting diodes (WLEDs) [21].

In recent years, researchers have extensively studied various glass matrices doped with Dy^{3+} ions. Recently, Chandrappa et al. using rare-earth (RE)-doped glass systems, they studied white light emission in a new glass composition and compared the results to those reported for trivalent Dy^{3+}-activated non-crystalline glasses for devices emitting white light and visible displays [22]. Thabit et al. studied the physical, optical, and spectroscopic properties of trivalent Dy^{3+}ion-incorporated borate glasses to achieve improved luminescence and radiative properties for potential use in laser platforms, and display screens [23]. Raj et al. investigated the possibility of white light emission under ultraviolet excitation in trivalent Dy^{3+}ion-doped lithium fluoro boro telluro phosphate glasses at different dopant concentrations [24]. Kashif et al. developed zinc boro tellurite glasses activated with varying concentrations of dysprosium oxide and discussed their optical and physical properties for potential application in optoelectronics [25]. Kuwik et al. investigated the influence of glass formers and modifiers on the luminescence properties of lead-free borate non-crystalline glasses activated with trivalent Dy^{3+} ions, which showed visible luminescence and could be potential yellowish emitters [26]. The study conducted by Abdullahi et al. investigated the impact of incorporating CuO nanoparticles on the enhancement of up-conversion emission and nonlinear optical characteristics in a multicomponent telluroborate glass matrix doped with trivalent Dy^{3+} ions [27]. Using constant lithium silicate concentrations, Kashif et al. studied the effects of replacing boron with RE Dy^{3+}ions [28]. In their study for white LEDs, Poojha et al. examined the effect of modifiers on their radiation properties of Dy^{3+}ion-included $B_2O_3+PbO+TeO_2+P_2O_5+Li_2O$ glasses [29]. For W-LED applications Murthy et al. investigated luminescence properties of Dy^{3+}ion-doped alumino-tungsten borate glasses [30]. Extensive research has been conducted on the luminescence properties and potential applications of dysprosium-doped glasses. Our investigation of Dy^{3+}-doped zinc phosphate glasses is driven by the need for more research in this field for white light emission applications, in order to advance solid-state lighting and optoelectronics. The primary objective of this study is to find out the possibility of zinc phosphate glasses with varying Dy^{3+}ion concentrations for usage in white light emission-requiring applications. This was accomplished by examining the spectral and structural characteristics of Dy^{3+} ions.

Experimental

Glass synthesis

In the current study, the glasses were fabricated utilizing a traditional melt-quenching method employing high-purity raw materials, specifically LiF (99.9%), SrO (99.9%), ZnO (99.9%), P_2O_5 (99.9%), and Dy_2O_3 (99.9%). The glass compositions are denoted as (60-n)P_2O_5-20ZnO-10SrO-10LiF-nDy_2O_3, with x ranging from 0.1 to 2.0%. The components of the batch were measured based on their stoichiometric ratios, and the compounds were initially thoroughly mashed for a duration of 30 min using an agate mortar and pestle until achieving a state of homogeneity. The mixer was then shifted to an aluminum crucible and kept in an Indfurr high-temperature programming furnace operated at 440v set at 1150 °C for 1 h to attain homogeneous melting [22]. This step ensured that the compounds were fully mixed and fused together. The homogeneous melt was then quenched on a brass plate and squeezed through another brass plate for samples ZnP01Dy, ZnP05Dy, ZnP10Dy, ZnP15Dy, and ZnP20Dy, as listed in Table 1. The quenching process prevented the crystallization of the melt and produced amorphous samples. The acquired samples underwent annealing at a temperature of 300 °C for a duration of 3 h in order

Table 1 Glass composition of Dy^{3+} ions-incorporated ZnP glasses, and labels

Glass system	Composition (mol%)				
	P_2O_5	ZnO	SrO	LiF	Dy_2O_3
ZnP01Dy	59.9	20	10	10	0.1
ZnP05Dy	59.5	20	10	10	0.5
ZnP10Dy	59.0	20	10	10	1.0
ZnP15Dy	58.5	20	10	10	1.5
ZnP20Dy	58.0	20	10	10	2.0

to alleviate any internal stress resulting from rapid cooling. The glass samples that have been prepared are depicted in Fig. 1.

Characterisation techniques

At standard room temperature, index of refraction (n) of glass was determined by using an Abbe model ATAGO refractometer that was equipped with a wavelength of 589.3 nm. The contact liquid used for this measurement was 1-bromonaphthalene. In general, the densities (ρ) of all ZnP glasses doped with Dy^{3+} ions were estimated using Archimedes' principle with oxidane (ρ = 0.999 gm/cm^3) as the immersion liquid. To measure the density, the glass samples were weighed using a Shimadzu BL220H electronic weighing balance in air and oxidane. To determine whether the Dy^{3+} ion-doped ZnP glasses were crystalline or amorphous, a RIGAKU benchtop model mini flex 600 X-ray diffractometer operated at 40 kV and 15 mA was used. The imaging of specimens through the use of scanning electron microscopy involves the utilization of the JEOL-manufactured JSM-IT 500 MODEL, which is outfitted with the AMTEX Energy Dispersive Spectroscopy (EDS) device. Fourier transform infrared spectroscopy (FTIR) measurements were performed in the spectral range of 400 cm^{-1}to 4000 cm^{-1} using a Perkin Elmer FTIR spectrometer with a resolution of 0.5 cm^{-1}. The Raman spectrum was acquired by a Renishaw Metrological Systems UK model: Invia Reflex Laser Confocal Raman Microscope with Spectrometer in the range between 50 cm^{-1} and 1500 cm^{-1}. At a resolution of 1 nm, UV-Vis-NIR absorption spectra in the 200–1800 nm range were measured using a Shimadzu UV3600 Plus spectrophotometer. To perform excitation, and emission studies, a Horiba Jobin Yvon Fluorolog FL3-11 spectrofluorometer was used with a 450 W xenon lamp, UV-visible source.

Results and discussion

Physical and optical properties

As shown in Fig. 1, the fabricated ZnP glasses were pale yellow in colour, had good transparency, and a smooth surface for physical appearance. The indices of refraction (n) and densities (ρ) of ZnP glasses doped with different Dy^{3+} concentrations are important parameters for evaluating their optical quality and structural stability. In this study, the refractive indices, and densities of five ZnP glasses with Dy^{3+} concentrations of 0.1, 0.5, 1.0, 1.5 and 2.0 mol% were measured. Table 2 presents the results. One of the parameters that can reveal the structural changes in glassy materials is density [28]. As shown in Fig. 2, the density (ρ) of the glasses increased with increasing Dy_2O_3 concentration. This may be due to the replacement of the lower molecular weight (M.W) component P_2O_5 (141.95 g/mol) by the higher

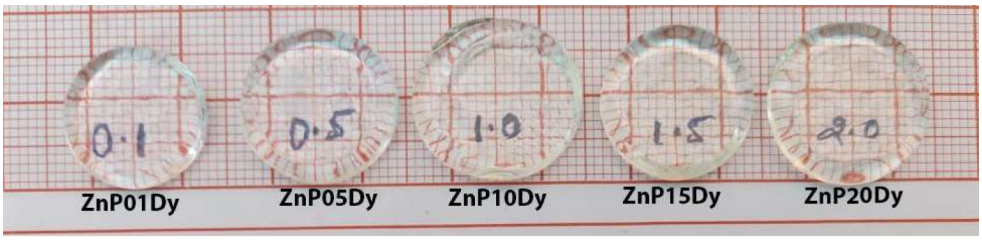

Fig. 1 Photographs of prepared glass samples

Table 2 Important physical and optical properties of prepared Dy^{3+} ions-incorporated ZnP glasses

Property	ZnP01Dy	ZnP05Dy	ZnP10Dy	ZnP15Dy	ZnP20Dy
Refractive Index (n)	1.654	1.653	1.654	1.654	1.653
Thickness t (cm)	0.272	0.284	0.286	0.280	0.275
Density (gm/cm^3)	2.686	2.961	3.165	3.223	3.296
Molecular Weight M.W (gm/mol)	114.62	115.55	116.70	117.86	119.01
Ion Concentration (N×10^{20} ion/cm^3)	0.14	0.77	1.63	2.47	3.34
Molar Volume V_m (cm^3/mol)	42.68	39.02	36.87	36.57	36.11
Molar Refraction R_m (cm^{-3})	15.64	14.29	13.51	13.40	13.22
Inter Atomic Distance (Å×10^{20})	1.92	1.09	0.85	0.74	0.67
Oxygen Packing Density (OPD, mol/cm^3)	77.28	84.31	88.95	89.42	90.28
Metallization factor (M)	0.63	0.63	0.63	0.63	0.63

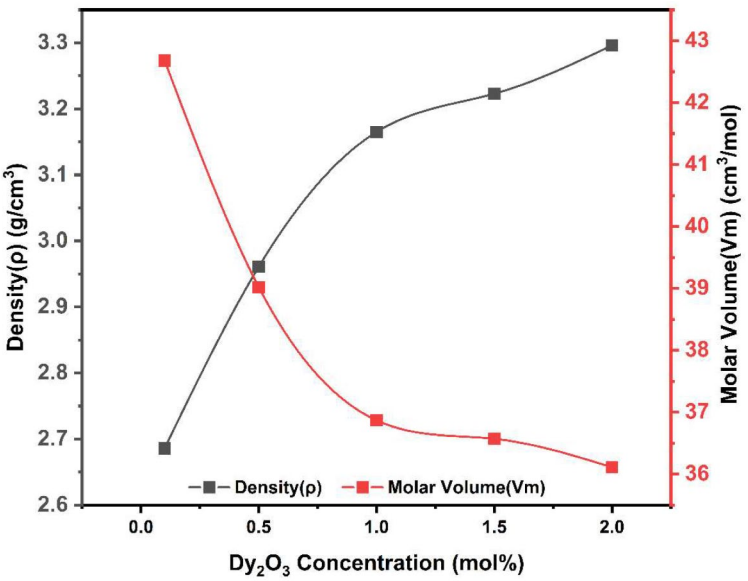

Fig. 2 Variation of Density and molar volume w.r.to Dy_2O_3 concentration

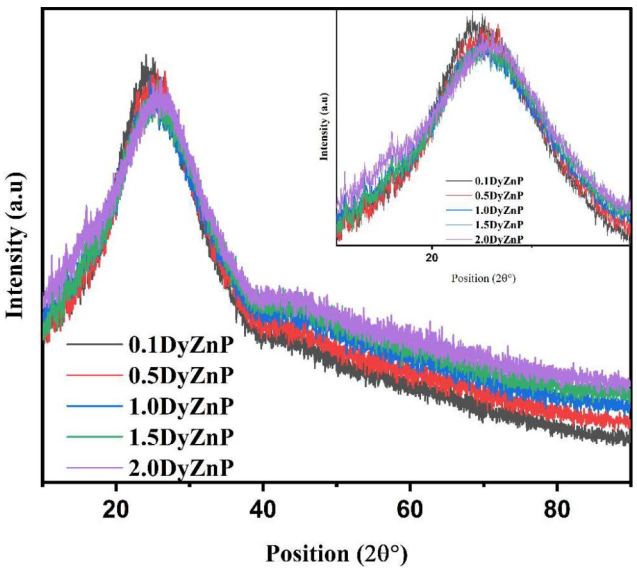

Fig. 3 XRD profiles of Dy^{3+}ion-incorporated ZnP glasses of different concentrations with broad humps (inset)

molecular weight (M.W) component Dy_2O3 (372.99 g/mol). This suggests that the glass network become stiffer and dens [31]. The molar volume (V_m) provides information about the structural changes and compactness of glass structure [32]. In this study, the molar volume decreases with increasing Dy_2O_3 concentration. This observation suggests that glasses containing higher concentrations of Dy_2O_3 have higher oxygen packing density (OPD) and lower interatomic distance [33]. From the refractive index (n) and density (ρ) values using the equations reported in the literature [34], several important properties of the ZnP glasses were calculated. The obtained values are presented in Table 2. The observed values of the prepared ZnP glasses suggest that the presence of Dy^{3+} ions have an influence on these properties.

X-ray powder diffraction analysis

Figure 3 illustrates the X-ray powder diffraction (XRD) patterns of ZnP glasses at ambient temperature, where the glasses are doped with different amounts of Dy^{3+} ions. In this case, there was no sharp peak corresponding to any crystalline phase in the XRD patterns, except for a broad hump around $2\theta = 10°\text{-}40°$. This hump, which is characteristic of amorphous materials, shows that the glass network has short-range order [35]. Therefore, this result confirms that the prepared glasses have an amorphous nature and show no crystallization owing to doping with Dy^{3+} ions.

SEM-EDX analysis

The morphology of the synthesized ZnP20Dy glass was examined by scanning electron microscopy (SEM). Figure 4 (a) shows an SEM image of a representative sample. The image shows that the glass had a smooth surface and there was no evidence of crystallinity. This observation suggests that the doping procedure did not alter the amorphous characteristics of the glass matrix. The smooth surface also implies that the glass has a good optical quality and homogeneity. Figure 4 (b) shows the results of the energy dispersive X-ray spectroscopy (EDX) analysis performed on the ZnP20Dy glass sample and provides valuable information about its elemental composition. Figure 4 (b) shows the peaks for zinc (Zn), phosphorus (P), oxygen (O), strontium (Sr), fluoride (F), and dysprosium (Dy) at their respective energies. This indicates the presence of elements in the

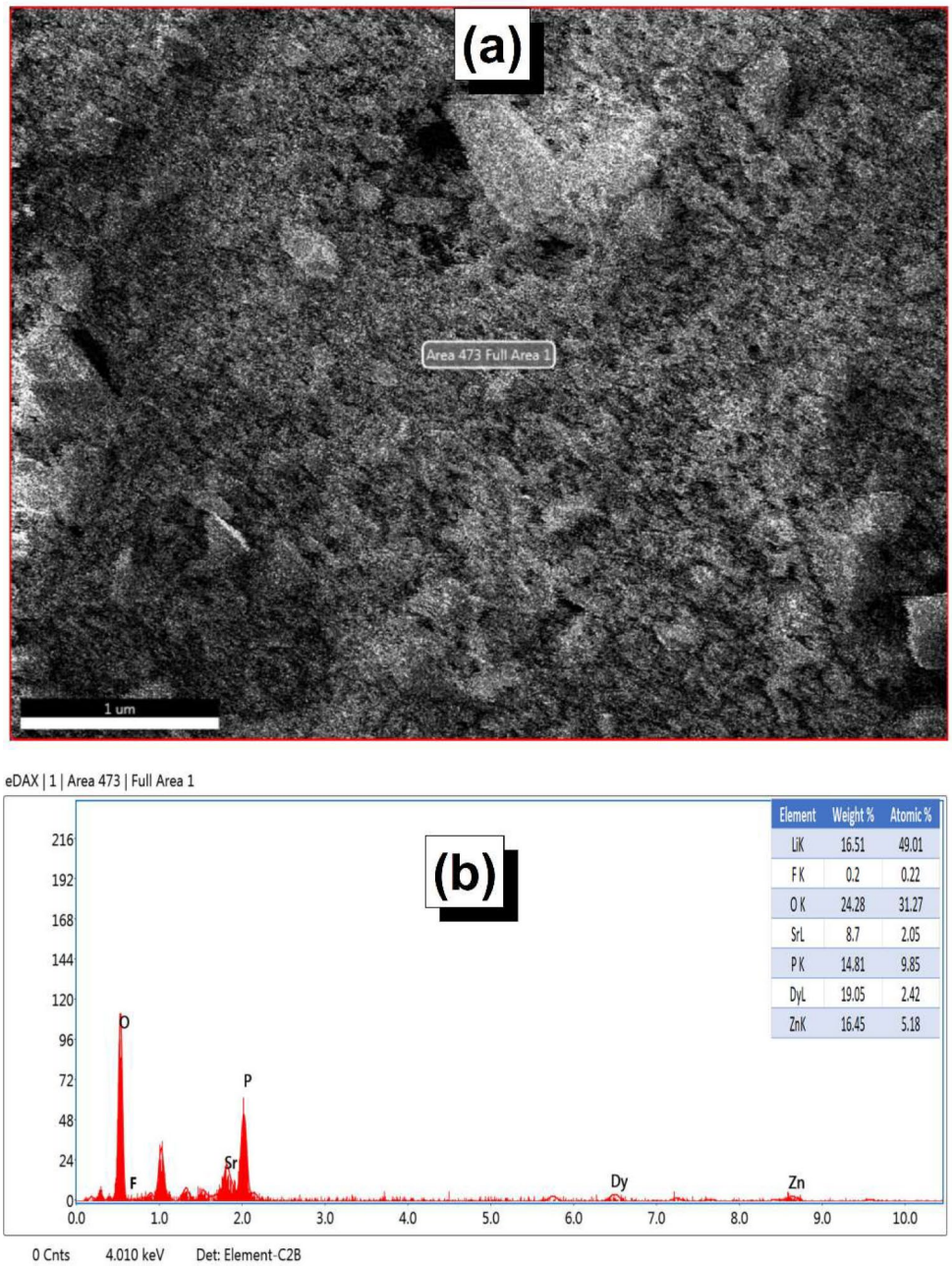

Fig. 4 **a**) Representative SEM image **b**) EDX of the ZnP20Dy glass sample along with the percentages of elements present

composition by displaying the characteristic X-ray peaks for each element. The inset of Fig. 4 (b) presents a quantitative analysis of the elements present in wt% and atomic % obtained from the EDX spectrum. These results are in agreement with the nominal compositions of the glass samples.

Fourier transform infrared and Raman analysis

At ambient temperature, as illustrated in Fig. 5, a total of seven peaks were detected in the FTIR spectra of ZnP glasses incorporating varying quantities of Dy^{3+} ions. The positions and corresponding assignments of these peaks are presented in Table 3. Of the seven peaks, four were in the fingerprint region, and four were in the functional group region. The harmonic P-O-P symmetric bending vibration, along with the Zn-O vibration, is responsible for the band (a) between 500 and 519 cm^{-1} [1, 29, 36]. Band (b) between 754 and 762 cm^{-1}, and band (c) between 921 and 925 cm^{-1} are ascribed to the asymmetric stretching vibration of the P-O-P linkages in Q^1 tetrahedra with (non-bridging oxygen atoms) NBOs in $(PO4)^{-2}$ and Q^2 tetrahedra in $(PO_4)^{-1}$, respectively [1, 36]. The asymmetric stretching vibration of the $P\text{-}O^-$ bonds, which are produced from the phosphorous non-bridging oxygen fraction of the tetrahedra, is detected

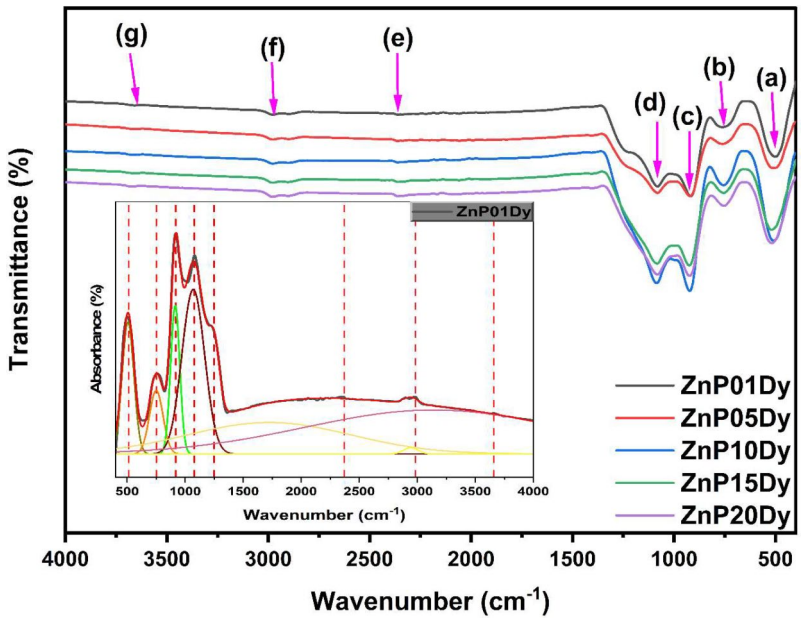

Fig. 5 FTIR Spectra of different concentration of Dy^{3+}ion-incorporated ZnP glasses

Table 3 Observed peak positions (cm^{-1}) and their assignments to FTIR spectra of Dy^{3+} ions-incorporated ZnP glasses

Band	Wave number (cm^{-1})					Assignment
	ZnP01Dy	ZnP05Dy	ZnP10Dy	ZnP15Dy	ZnP20Dy	
a	500	508	509	519	518	ν_s(P-O$^-$) & Zn-O bonds[1, 29, 35]
b	762	761	755	755	754	ν_{as}(P-O-P) linkages of Q^1 tetrahedra in $(PO_4)^{-2}$[1, 35]
c	921	921	923	925	925	ν_{as}(P-O-P) linkages of Q^2 tetrahedra in $(PO_4)^{-1}$[1, 35]
d	1081	1081	1085	1083	1081	ν_{as}(P-O$^-$) bonds influenced by ZnO [8, 35–37]
e	2362	2363	2364	2360	2362	OH, groups strongly bonded to the phosphorus atoms [8, 19]
f	2975	2976	2978	2977	2977	Small stretching vibrations P-O-H bonds [1, 8, 35]
g	3661	3665	3661	3664	3665	Water molecules, small free OH groups [8, 35]

between 1081 and 1085 cm^{-1}, and band (d) is influenced by the ZnO content in the glass system [7, 36–38]. The infrared spectra of the samples also showed three distinct bands (e), (f), and (g), which are related to the presence of hydroxyl groups. 2364 cm^{-1} located between 2360 and 2364 cm^{-1}, may be due to the hydrogen bond between O-Zn [19] and the OH groups that are strongly bonded to the phosphorus atoms [7]. The stretching vibrations of the P-O-H bonds are responsible for band (f), which was found between 2975 and 2977 cm^{-1} [1, 7, 36]. The band (g) appearing between 3661 and 3665 cm^{-1}, indicates the existence of free OH groups that are not attached to any other atom [7, 36]. Based on the FTIR spectra, Dy^{3+} ions influenced the glass structure. Although the spectra did not directly show dysprosium, they indicated the presence of Dy_2O_3. Increased Dy_2O_3 did not change the number of bands in the spectra but slightly changed their position and intensity [1]. This is caused by the formation of NBOs when some of the matrix elements are replaced by Dy^{3+} ions.

Figure 6 shows the deconvoluted Raman spectrum of ZnP glass doped with 2.0 mol% Dy^{3+} ions. The observed spectrum shows six distinct bands in the frequency range of 100 cm^{-1} 1500 cm^{-1}, which can be attributed to several vibrational modes associated with the glass network. Table 4 presents the peak positions and corresponding assignments. The occurrence of the Raman band at Raman shift 347 cm^{-1} was attributed to the oscillation in Zn-O bonds, specifically related to bending vibrations [7]. The presence of the shoulder at 566 cm^{-1} may be ascribed to the asymmetric bending vibration of the P-O bonds within the pyro (Q^1) and meta phosphate (Q^2) units [14]. The 738 cm^{-1} Raman band corresponds to the symmetric stretching vibration of the P-O-P bonds in the Q^1 structure [36, 39]. The presence of NBOs within the smaller meta phosphate units (Q^2) causes the asymmetric stretching vibration of the P-O-P bonds observed at 1050 cm^{-1} [36, 39]. The peak observed at 1139 cm^{-1} is attributed to the symmetric stretching vibration of NBOs within the O-P-O metaphosphate unit (Q^1) [14, 39]. Similarly, the band at 1247 cm^{-1} is associated with the symmetric stretching vibration of NBOs in the pyro phosphate (Q^1) unit [7]. In conclusion, the Fourier transform IR spectra of the Dy^{3+} ions-incorporated ZnP glasses showed vibration bands that aligned with the distinctive zinc and phosphate groups, as confirmed by Raman analysis.

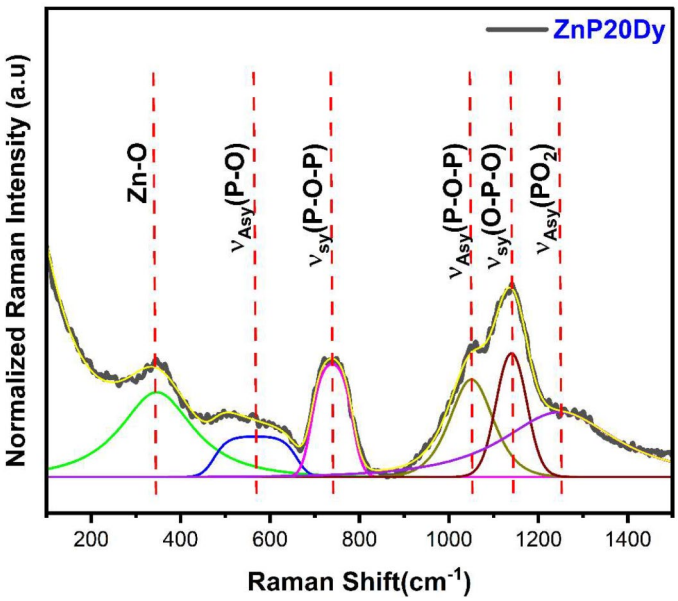

Fig. 6 Representative Deconvoluted Raman spectra of ZnP20Dy glass samples

Table 4 Peak position (cm^{-1}) and their assignments to the Raman spectrum of the ZnP20Dy glass sample

Raman Shift (cm^{-1})	Peak Assignment
347	Zn-O bonds[8]
566	ν_{Asy}(P-O) bonds in pyro/meta phosphate groups[6]
738	ν_{sy}(P-O-P) bonds in meta phosphate groups [35, 38]
1050	ν_{Asy}(P-O-P) bonds in meta phosphate groups [35, 38]
1139	ν_{sy} (O-P-O) bonds in meta phosphate groups [6, 38]
1247	ν_{Asy}(PO_2) bonds in pyro phosphate groups [8]

Analysis of optical absorption spectra

Figure 7 depicts the ambient temperature ultraviolet-visible-near-infrared absorption spectra of different concentrations of Dy^{3+} ions-incorporated ZnP glasses. As shown in Fig. 7, the strength and number of absorption bands increased with increasing Dy_2O_3 concentration. The spectra show nine distinct bands corresponding to the electronic transitions of Dy^{3+} ions from the $^6H_{15/2}$ ground state to different excited states such as "$^4I_{11/2}$ (360 nm), $^4I_{13/2}$+$^4F_{7/2}$ (385 nm), $^4G_{11/2}$ (424 nm), $^4I_{15/2}$ (450 nm), $^4F_{9/2}$ (472 nm), $^6H_{5/2}$+$^6F_{7/2}$ (896 nm), $^6H_{7/2}$+$^6F_{9/2}$ (1090 nm), $^6H_{9/2}$+$^6F_{11/2}$ (1269 nm), and $^6H_{11/2}$ (1690 nm)" [40]. Among these transitions, the $^6H_{15/2}$ → $^6H_{9/2}$+$^6F_{11/2}$ (1269 nm) transition in the NIR region is high in intensity and is referred to as hypersensitive transition (HST) [41, 42] which obey the selection rules ‖ΔS‖=0, ‖ΔL‖≤2, ‖ΔJ‖≤2 [13, 27] and is sensitive to the changes in the symmetry and the ligand field of the Dy^{3+} ions [29].

Nephelauxetic ratio (β) and bonding parameter (δ)

The absorption spectra offer valuable insights into the bonding characteristics between RE ions and ligand oxygens in the host network [29]. Table 5 shows the results of calculating the nephelauxetic effect (β) and bonding parameter (δ) values based on the partially filled f-shell of the Dy^{3+}ion-doped ZnP glasses using formulae from the literature [32, 43]. The bonding parameter (δ) is a pivotal tool that serves as an indicator of the type of bond, distinguishing between covalent (positive values) and ionic (negative values) [16, 38]. The bonding parameter (δ) values obtained in this study were negative, suggesting that Dy^{3+} ions formed ionic bonds with the ligands present in all glass matrices [16].

Analysis of Bandgap energy and Urbach energy

The study of the optical bandgap (E_g) and Urbach energy (E_U) values is crucial for understanding electronic transitions in amorphous materials [44]. The optical bandgap (E_g) is a vital factor in explaining the absorption properties of a material, which are essential for optoelectronic applications [45]. On the other hand, Urbach energy (E_U) is a critical optical parameter for amorphous materials, providing information on the disorderliness of glass samples [24]. Here, we utilized Tauc's method, as described in the literature [46], to determine the direct and indirect allowed bandgap and Urbach energy values. As depicted in Fig. 8(a) and 8(b), Tauc's plots were employed to evaluate both the direct and indirect allowed optical bandgaps. The measured optical band gap values are listed in Table 6. The optical band gap energies (direct (E_g^{Direct}) and indirect ($E_g^{Indirect}$))

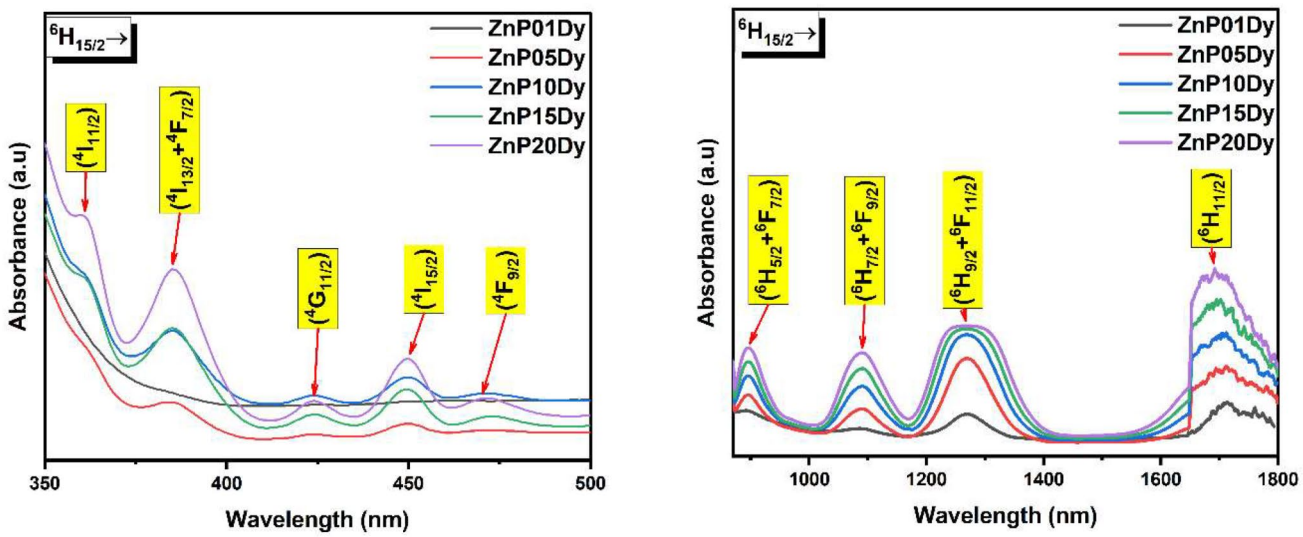

Fig. 7 Absorption spectra of different concentrations of Dy^{3+}-incorporated ZnP glasses in UV-VIS-NIR regions

Table 5 Average nephelauxetic ratio ($\overline{\beta}$) and bonding parameters (δ) of prepared Dy^{3+} ions-incorporated ZnP glasses

Transition	ZnP01Dy	ZnP05Dy	ZnP10Dy	ZnP15Dy	ZnP20Dy	ν_{aqu}
$^6H_{11/2}$	05820	05896	05896	05913	05917	05833
$^6H_{9/2}$+$^6F_{11/2}$	07874	07867	07867	07874	07905	07700
$^6H_{7/2}$+$^6F_{9/2}$	09170	09212	09170	09170	09174	09100
$^6H_{5/2}$+$^6F_{7/2}$	11,160	11,166	11,160	11,160	11,154	11,000
$^4F_{9/2}$	-	21,321	21,321	21,141	21,231	21,100
$^4I_{15/2}$	-	22,222	22,246	22,271	22,222	22,100
$^4G_{11/2}$	-	23,584	23,584	23,584	23,584	23,400
$^4I_{13/2}$+$^4F_{7/2}$	-	26,041	25,974	25,974	25,974	25,800
$^4I_{11/2}$	-	-	27,855	27,777	27,777	27,503
$\overline{\beta}$	1.01	1.01	1.01	1.01	1.01	
δ	-0.99	-0.99	-0.99	-0.99	-0.99	

for the zinc phosphate glasses under study decreased from 3.350 to 3.272 eV and from 3.217 to 3.142 eV, respectively. This bandgap (E_g) reduction is attributed to the structural network changes caused by the incorporation of Dy^{3+} ions into the ZnP glasses. The increase in Dy_2O_3 concentration and decrease in P_2O_5 concentration in the glass system leads to an increase in localized electrons, resulting in the transition of donors to centers. This results in an increase in NBOs and a potential decrease in the bandgap. The ZnP01Dy glass possessed higher direct (E_g^{Direct}) and indirect ($E_g^{Indirect}$) band gap energies of 3.350 and 3.217 eV, respectively, whereas the ZnP20Dy glass exhibited lower direct (E_g^{Direct}) and indirect ($E_g^{Indirect}$) band gap energies of 3.236 and 3.142 eV, respectively. The Urbach energy (E_U) of the glasses was determined by plotting hυ against ln(α) [46], as demonstrated in Fig. 8(c). The slope value obtained from the linear fit of the linear portion of hυ against ln(α) plot was inverted to obtain Urbach's energy values [13], which are presented in Table 6. As the concentration of Dy_2O_3 in the glass matrix increased from 0.1 to 2.0 mol%, the energy levels of Urbach progressively increased from 0.864 to 1.219 eV. Specifically, the ZnP01Dy glass had a lower Urbach energy of 0.864 eV, while the ZnP20Dy glass had a higher Urbach energy of 1.219 eV The increase in Urbach energy suggests an increase in the disorder of the glass samples [19].

Analysis of Judd-Ofelt (JO) intensity parameters

Using the JO theory, the oscillator strengths (experimental (f_{exp}) and theoretical (f_{th})), and root mean square (δ_{RMS}) deviations of the present Dy^{3+}-incorporated ZnP glasses were calculated using equations reported elsewhere in the existing literature [43]. The obtained values of the oscillator strengths (f_{exp} *and* f_{th}) and root mean square (δ_{RMS}) deviations are presented in Table 7. From Table 7, it is evident that the transition from $^6H_{15/2}$ to $^6H_{9/2}$+$^6F_{11/2}$ (HST) has the highest values of oscillator strength (f_{exp} and f_{th}) among all

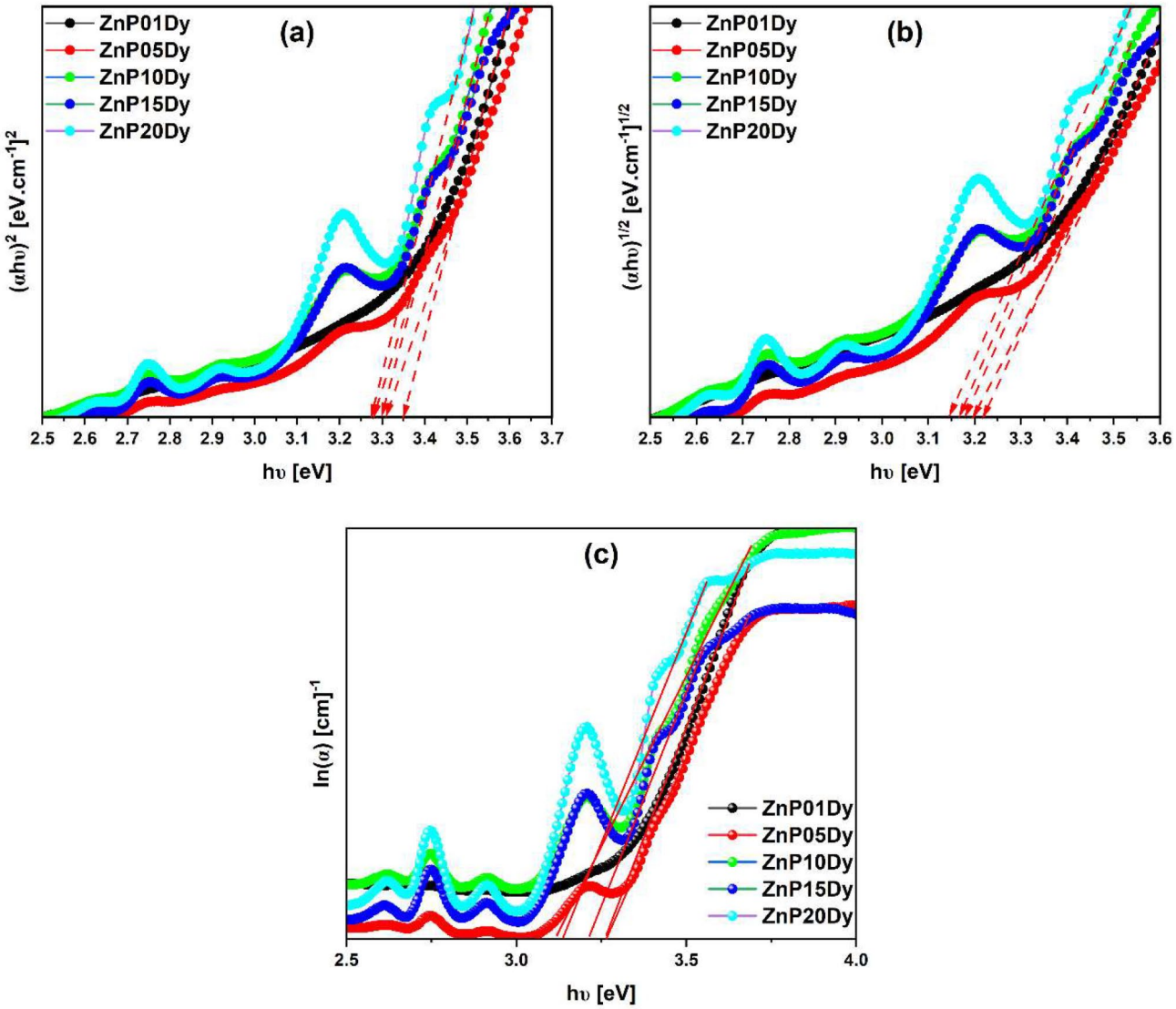

Fig. 8 Tauc's plot for **a**) direct bandgap **b**) indirect bandgap and **c**) Urbach's plot for different concentrations of Dy^{3+} ion-incorporated ZnP glasses

Table 6 Direct bandgap energy (E_g^{Direct}, eV), indirect bandgap energy ($E_g^{Indirect}$, eV) and Urbach energy ($E_{U,}$ eV) of prepared Dy^{3+} ions-incorporated ZnP glasses

Glass System	E_g^{Direct} (eV)	$E_g^{Indirect}$ (eV)	E_U (eV)
ZnP01Dy	3.350	3.217	0.864
ZnP05Dy	3.310	3.194	0.993
ZnP10Dy	3.298	3.178	1.094
ZnP15Dy	3.280	3.168	1.199
ZnP20Dy	3.272	3.142	1.219

the transitions in the prepared ZnP glasses. It should also be noted that the ZnP01Dy glass has high oscillator strengths (f_{exp}*and* f_{th}) compared with the other glasses studied. Low δ_{RMS} deviation values were obtained for the ZnP glasses, indicating a good agreement between the experimental (f_{exp}) and theoretical (f_{th}) oscillator strengths [16]. It also shows the accuracy of the JO intensity parameters [47].

Three phenomenological JO intensity parameters were determined by fitting the experimental and theoretical oscillator strengths (f_{exp} and f_{th}) to determine the environment around the RE ions and their interactions with the glass host [48]. The obtained results are presented in Table 8. In general, the short-range coordination effects associated with Ω_2 describe the covalency and asymmetry of the ligand field located precisely around the RE ion site [22], while

Table 7 Experimental and theoretical oscillator strengths (f_{exp} and f_{th} $\times 10^{-6}$, cm^2) and root mean square deviations ($\delta_{RMS} \times 10^{-6}$) of Dy^{3+} ions-incorporated ZnP glasses

Energy Level $^6H_{15/2}\rightarrow$	ZnP01Dy		ZnP05Dy		ZnP10Dy		ZnP15Dy		ZnP20Dy	
	f_{exp}	f_{th}	f_{exp}	f_{th}	f_{exp}	f_{th}	f_{exp}	f_{th}	f_{exp}	f_{th}
$^6H_{11/2}$	4.76	4.20	2.96	2.63	2.21	1.97	1.89	1.59	1.96	1.61
$^6H_{9/2}+^6F_{11/2}$	11.16	11.24	6.69	6.73	4.76	4.80	3.85	3.90	3.99	4.04
$^6H_{7/2}+^6F_{9/2}$	8.42	8.09	4.51	4.39	3.29	3.22	2.69	2.61	2.82	2.70
$^6H_{5/2}+^6F_{7/2}$	6.91	8.23	4.14	4.87	3.11	3.64	2.25	2.93	2.20	2.99
$^4F_{9/2}$	-	-	1.06	0.38	0.92	0.29	0.95	0.23	0.91	0.23
$^4I_{15/2}$	-	-	1.30	0.98	1.01	0.73	1.07	0.59	1.08	0.60
$^4G_{11/2}$	-	-	1.20	0.02	0.90	0.01	0.97	0.01	1.07	0.01
$^4I_{13/2}+^4F_{7/2}$	-	-	2.15	0.93	1.85	0.67	2.22	0.55	2.20	0.58
$^4I_{11/2}$	-	-	-	-	1.16	0.09	1.04	0.00	1.18	0.08
δ_{RMS}	±0.74		±0.71		±0.68		±0.81		±0.85	

Table 8 Judd-Ofelt (JO) intensity parameters (Ω_2, Ω_4, $\Omega_6 \times 10^{-20}$, cm^2) and their trend in present studied ZnP glasses along other reported values of Dy^{3+} ions incorporated glasses

Glass System	JO intensity parameters			Trend
	Ω_2	Ω_4	Ω_6	
ZnP01Dy [Present]	8.95	2.19	9.90	$\Omega_6 > \Omega_2 > \Omega_4$
ZnP05Dy [Present]	6.04	0.32	6.22	$\Omega_6 > \Omega_2 > \Omega_4$
ZnP10Dy [Present]	4.43	0.07	4.55	$\Omega_6 > \Omega_2 > \Omega_4$
ZnP15Dy [Present]	3.60	0.10	3.65	$\Omega_6 > \Omega_2 > \Omega_4$
ZnP20Dy [Present]	3.64	0.23	3.70	$\Omega_6 > \Omega_2 > \Omega_4$
TeO_2–ZnF_2–Pb_2O_5–Nb_2O_5–Dy_2O_3[50]	2.32	0.64	4.64	$\Omega_6 > \Omega_2 > \Omega_4$
ZrF_4–BaF_2–AlF_3–NaF–LaF_3-Dy_2O_3[51]	1.86	1.42	2.37	$\Omega_6 > \Omega_2 > \Omega_4$
Gd_2SiO_5: 5 at.%Dy^{3+}(GSO)[52]	3.22	2.16	3.76	$\Omega_6 > \Omega_2 > \Omega_4$
OFLZBSD1.0[53]	2.42	0.80	2.65	$\Omega_6 > \Omega_2 > \Omega_4$

the long-range coordination effects associated with Ω_4 and Ω_6 describe bulk properties such as stiffness, viscosity, and basicity [23, 35, 49]. A similar trend was observed in the resulting JO intensity parameters for all the produced Dy^{3+}-incorporated ZnP glasses: $\Omega_6 > \Omega_2 > \Omega_4$. The results were subsequently compared to those observed in other glasses doped with Dy^{3+}, exhibiting a similar pattern [50–53], as indicated in Table 8. It was found that the magnitude of Ω_2 for the system under analysis was significantly greater than Ω_4 but less than Ω_6. According to the data presented in Fig. 9, it can be observed that the magnitudes of Ω_2 and Ω_6 decreased with increasing concentration of Dy^{3+}ions and reached a maximum decrease at a concentration of 1.5 mol%. Nevertheless, the values of Ω_2 and Ω_6 increased as the concentration of Dy^{3+} was increased further. High rigidity and low polarizability of the ligands are indicated by the higher magnitudes of Ω_6 obtained [53, 54]. Table 8 shows that the ZnP01Dy glass has the highest covalency nature and high asymmetry of the ligands located precisely around the dysprosium ions.

Radiative properties

Laser properties such as radiative transition rates (A_T), calculated branching ratios (β_{cal}), absorption cross-sections (σ_{abs}), and calculate radiative lifetimes (τ_{rad}) of various Dy^{3+} ion transitions are computed using refractive index and JO intensity parameters [55]. The equations used for these calculations are provided in the literature [34]. The results are presented in Tables 9 and 10, respectively. The most prominent $^6F_{5/2}\rightarrow{}^6F_{7/2}+^6H_{5/2}$ transition has the highest total transition probability (A_T) for all glasses, indicating strong radiative emission. The magnitudes of A_T of the other transitions followed the order $^6F_{7/2}+^6H_{5/2}>{}^4F_{9/2}>{}^6F_{3/2}>{}^6H_{11/2}>{}^6F_{5/2}$ for all the glasses. The total transition probability (A_T) of the $^6F_{5/2}\rightarrow{}^6F_{7/2}+^6H_{5/2}$ transition varies with glass composition, such as ZnP01Dy > ZnP05Dy > ZnP10Dy > ZnP20Dy > ZnP15Dy. The magnitude of the branching ratios (β_{cal}) of the $^4F_{9/2}\rightarrow{}^6H_{13/2}$ transition was high for all glasses, suggesting a high probability of yellow emission. The magnitude of σ_{abs} of the $^4F_{9/2}\rightarrow{}^6H_{13/2}$ transition was also high for all glasses, indicating strong absorption at this wavelength. The radiative lifetime (τ_{rad}) of the $^6F_{3/2}\rightarrow{}^6F_{5/2}$ transition was the highest for all glasses, implying a long-lived metastable state. The magnitudes of the radiative lifetimes (τ_{rad}) of the

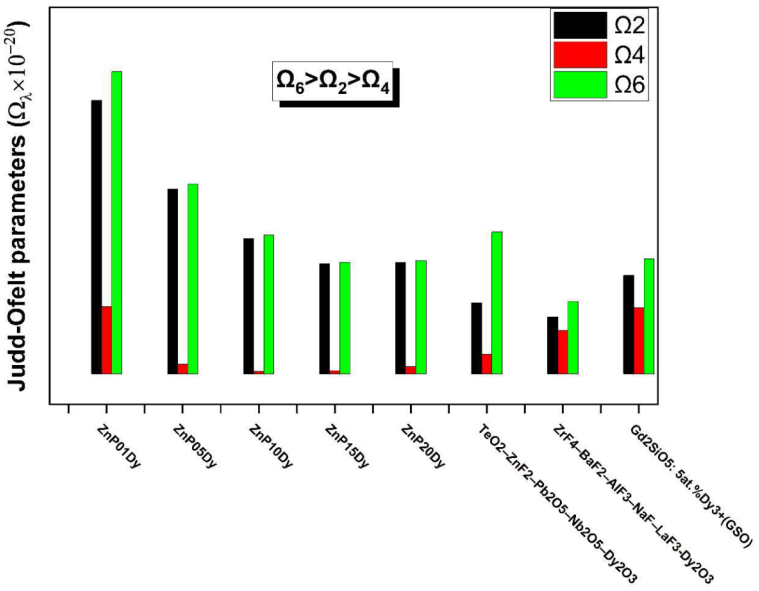

Fig. 9 Trend of Judd-Ofelt parameters in comparison with Dy^{3+} ion-incorporated reported glasses

Table 9 Radiative total transition probabilities (A_T, s^{-1}) and radiative lifetimes (τ_{rad}, μs) of certain excited states of Dy^{3+} ions-incorporated ZnP glasses

Glass System	$^4I_{15/2}\rightarrow{}^4F_{9/2}$		$^4F_{9/2}\rightarrow{}^6F_{3/2}$		$^6F_{3/2}\rightarrow{}^6F_{5/2}$		$^6F_{5/2}\rightarrow{}^6F_{7/2}+{}^6H_{5/2}$		$^6F_{11/2}+{}^6H_{9/2}\rightarrow{}^6H_{11/2}$	
	A_T	τ_{rad}	A_T	τ_{rad}	A_T	τ_{rad}	A_T	τ_{rad}	A_T	τ_{rad}
ZnP01Dy	1777	0562	1737	0575	1155	0865	1913	0522	1297	0770
ZnP05Dy	1088	0918	1101	0907	0685	1459	1098	0910	0770	1297
ZnP10Dy	0808	1236	0809	1235	0511	1955	0818	1221	0554	1804
ZnP15Dy	0656	1522	0639	1563	0412	2424	0660	1513	0446	2240
ZnP20Dy	0663	1507	0665	1502	0419	2386	0672	1486	0467	2138

Table 10 Calculated branching ratios (β_{cal}) and stimulated absorption cross-sections ($\sigma_{abs}\times10^{-18}$ cm^2) of prepared Dy^{3+} ions-incorporated ZnP glasses

Transitions $^4F_{9/2}\rightarrow$	ZnP01Dy		ZnP05Dy		ZnP10Dy		ZnP15Dy		ZnP20Dy	
	β_{cal}	σ_{abs}	β_{cal}	σ_{abs}	β_{cal}	σ_{abs}	β_{cal}	σ_{abs}	β_{cal}	σ_{abs}
$^6F_{3/2}$	0	0	0	0	0	0	0	0	0	0
$^6F_{5/2}$	0.004	0.05	0.005	0.03	0.005	0.02	0.005	0.02	0.005	0.02
$^6F_{7/2}+{}^6H_{5/2}$	0.008	0.07	0.008	0.04	0.008	0.03	0.008	0.03	0.008	0.03
$^6H_{7/2}+{}^6F_{9/2}$	0.02	0.12	0.017	0.06	0.016	0.04	0.016	0.04	0.017	0.04
$^6F_{11/2}+{}^6H_{9/2}$	0.029	0.14	0.028	0.08	0.027	0.06	0.027	0.05	0.028	0.05
$^6H_{11/2}$	0.046	0.17	0.048	0.11	0.047	0.08	0.047	0.06	0.047	0.06
$^6H_{13/2}$	0.592	1.61	0.605	1.03	0.602	0.75	0.602	0.6	0.601	0.62
$^6H_{15/2}$	0.301	0.57	0.289	0.34	0.295	0.26	0.295	0.2	0.294	0.21

other transitions followed the order $^6F_{5/2}>{}^6H_{11/2}>{}^6F_{3/2}>{}^4F_{9/2}>{}^6F_{7/2}+{}^6H_{5/2}$ for all the glasses. The radiative lifetime (τ_{rad}) of the $^6F_{3/2}\rightarrow{}^6F_{5/2}$ transition varies with glass composition, such as ZnP15Dy > ZnP20Dy > ZnP10Dy > ZnP05Dy > ZnP01Dy.

Analysis of excitation and emission spectra

The ambient temperature excitation spectra of ZnP glasses doped with Dy^{3+} ions, at a wavelength of 572 nm, are shown in Fig. 10(a). A total of eight transitional peaks were detected. The observed peaks in the spectrum can be attributed to the transition of Dy^{3+} ions from their ground state $^6H_{15/2}$ to several excited states, namely the states "$^4K_{15/2}+{}^6P_{3/2}$ (324 nm), $^4I_{9/2}$ (338 nm), $^4M_{15/2}+{}^6P_{7/2}$ (350 nm), $^4I_{11/2}$ (364 nm), $^4I_{13/2}+{}^4F_{7/2}$ (386 nm), $^4G_{11/2}$ (425 nm), $^4I_{15/2}$ (452 nm), and $^4F_{9/2}$ (473 nm)" [56]. Among the eight transition peaks, the $^6H_{15/2}\rightarrow{}^4M_{15/2}+{}^6P_{7/2}$ transition peak at a wavelength of 350 nm exhibited the highest intensity. As a

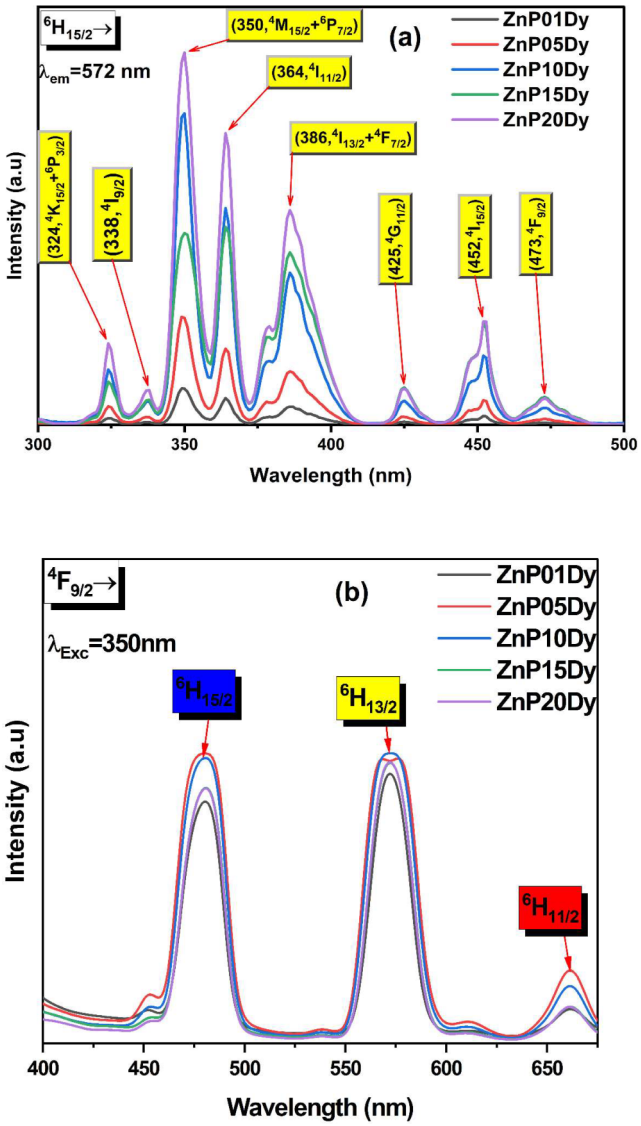

Fig. 10 **a**) Excitation **b**) Emission spectra of different concentrations of Dy^{3+}ion-incorporated ZnP glasses

result, the wavelength 350 nm was utilized as the excitation source to measure the emission spectra.

Figure 10(b) portrays the emission spectra of ZnP glasses doped with Dy^{3+} ions in the visible region at a wavelength of 350 nm under typical room temperature conditions. It is worth emphasizing that all the glass samples exhibited emission spectra with comparable profiles, as portrayed in Fig. 10 (b). without any noticeable displacement in the emission bands. Spectral analysis revealed two prominent bands and one less significant band in the visible region. According to the literature [57], blue, yellow, and red bands were observed namely, "($^4F_{9/2}\rightarrow{}^6H_{15/2}$: 481 nm), ($^4F_{9/2}\rightarrow{}^6H_{13/2}$: 572 nm), and ($^4F_{9/2}\rightarrow{}^6H_{11/2}$: 661 nm)", respectively. The blue band at 481 nm is unaffected by the local crystal field environment which is magnetic dipole (MD) transition [13, 58]. The yellow band at 572 nm which has the highest intensity among the three transition bands is an electric dipole (ED) transition and is referred to as the hypersensitive transition (HST), which obeys the selection rule ($\Delta J = 0, \pm 2$) [1, 13, 59]. The band at 661 nm which has a weak intensity in the red region is less significant [1, 38].

The luminescence intensity of RE ions is significantly influenced by the symmetry of the site where they are located, and there is an inverse relationship between the luminescence intensity and the site symmetry [53]. The yellow band at 572 nm has a higher intensity than the blue band at 481 nm, indicating that the ZnP glasses exhibit high site symmetry. The yellow-to-blue (Y/B) intensity ratio is largely affected by the local coordination environment near the Dy^{3+} ions and the inversion symmetry [59], which are reflected in the values presented in Table 11. The Y/B emission intensity ratio of Dy^{3+} ion must be equal to one for white light emission, and this is a crucial factor for classifying white light emission into warm, cool, or daylight regions [30]. As shown in Fig. 11, Y/B intensity ratios for all ZnP glasses is nearly equal to unity and are capable to generate the white light. In comparison to the reported DFBP [60], DP3 [19], BSLNAD5 [61], OFLZBSD0.1 [53], Dy05 [62], and NBZD05 [63] glass matrixes, Y/B intensity ratios of present ZnP glasses doped with Dy^{3+} ions were found to be low as listed in Table 11. As the concentration of Dy^{3+} ions increased, Yellow-to-blue (Y/B) intensity ratio also increased. The high covalency of Dy^{3+} ions were indicated by yellow-to-blue (Y/B) intensity ratio values greater than 1 [16, 18, 58]. The ZnP01Dy glass had the lowest Y/B value (1.11), whereas ZnP20Dy had the highest Y/B value (1.20), indicating the former's highest covalency [53]. This result is in line with the J-O intensity parameters in Table 8. From the emission spectra, for the three emission transitions, the emission wavelength peaks (λ_P), spontaneous emission rates (A_R), effective bandwidths ($\Delta\lambda_{eff}$), experimental branching ratios (β_{exp}), Peak stimulated emission cross-sections (σp), and gain bandwidths ($\Delta\lambda_{eff}\times\sigma p$) were calculated using the Füchtbauer–Ladenburg equation with the help of JO intensity parameters [43]. Table 12 presents the results. Peak stimulated emission cross-sections (σp) and branching ratios (β_{exp}) are two crucial factors that determine the laser properties of the synthesized glasses [16]. The presence of larger σp leads to an increased population inversion, a significant characteristic of laser gain medium [16]. Among the three transitions, the $^4F_{9/2}\rightarrow{}^6H_{13/2}$ transition of yellow band of all ZnP glasses exhibited a high A_R, $\Delta\lambda_{eff}$, β_{exp}, β_{cal}, and σp. Among all the prepared ZnP glasses doped with Dy^{3+} ions, ZnP01Dy glass exhibited a high σp for three transitions. Peak stimulated emission cross-sections (σp) for the aforementioned three transitions of ZnP01Dy glass are 0.72×10^{-21} cm^2, 2.85×10^{-21} cm^2 and 0.85×10^{-21} cm^2,

Table 11 Peak wavelength of emissions (λ_p, nm), effective bandwidths ($\Delta\lambda_{eff}$, nm), experimental branching ratios (β_{exp}, %), stimulated emission cross-sections ($\sigma p \times 10^{-21}$ cm^2), and gain bandwidths ($(\Delta\lambda_{eff} \times \sigma p) \times 10^{-25}$ cm^3) of $^4F_{9/2} \rightarrow {}^6H_{15/2}$, $^4F_{9/2} \rightarrow {}^6H_{13/2}$ and $^4F_{9/2} \rightarrow {}^6H_{11/2}$ transitions of present Dy^{3+} ions-incorporated ZnP glasses

	λ_P	A_R	$\Delta\lambda_{eff}$	β_{exp}	σp	$\Delta\lambda_{eff} \times \sigma p$
$^4F_{9/2} \rightarrow {}^6H_{15/2}$						
ZnP01Dy	481	522.8	12.29	45.93	0.72	0.009
ZnP05Dy	481	318.4	10.16	44.43	0.36	0.004
ZnP10Dy	481	238.8	10.12	44.10	0.27	0.003
ZnP15Dy	481	188.5	10.90	44.74	0.23	0.003
ZnP20Dy	481	195.4	11.10	43.90	0.24	0.003
$^4F_{9/2} \rightarrow {}^6H_{13/2}$						
ZnP01Dy	572	1027.7	17.46	51.03	2.85	0.050
ZnP05Dy	576	0666.6	12.72	49.99	1.37	0.017
ZnP10Dy	572	0487.1	12.62	50.85	0.98	0.012
ZnP15Dy	572	0385.1	14.49	52.22	0.89	0.013
ZnP20Dy	572	0400.4	14.43	52.67	0.92	0.013
$^4F_{9/2} \rightarrow {}^6H_{11/2}$						
ZnP01Dy	662	80.1	49.78	3.04	0.85	0.042
ZnP05Dy	661	53.0	38.34	5.58	0.43	0.017
ZnP10Dy	661	38.0	33.49	5.05	0.27	0.009
ZnP15Dy	662	30.0	34.87	3.76	0.22	0.008
ZnP20Dy	661	31.3	37.76	3.48	0.25	0.009

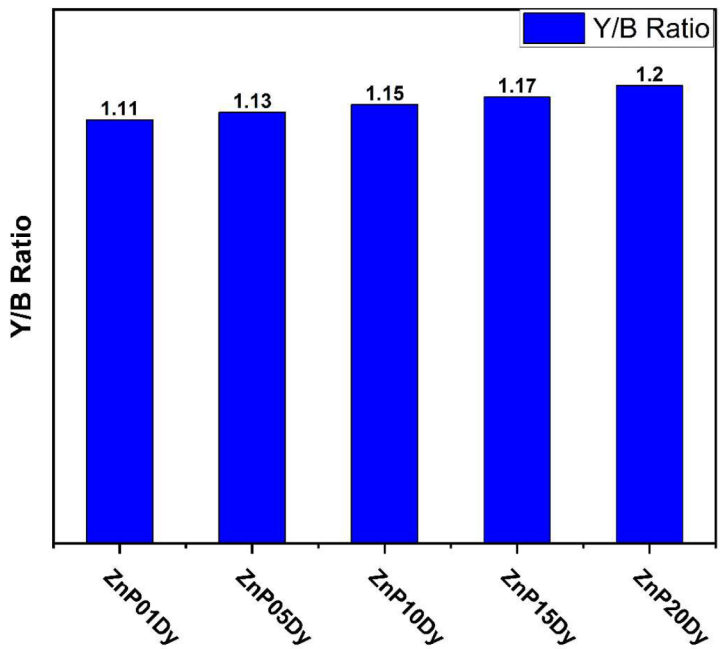

Fig. 11 Variation in the Y/B intensity ratio of different concentrations of Dy^{3+}ion-incorporated ZnP glasses

respectively. The obtained results indicate that ZnP01Dy glass exhibits higher A_R, $\triangle\lambda_{eff}$, σp, $(\Delta\lambda_{eff} \times \sigma p)$ and a small value of Y/B intensity ratio, suggesting its potential appropriateness for lasing applications and white light emitting devices.

Colorimetry

The determination of the exact colour emitted by prepared glasses using CIE 1931 colour coordinates (x_c, y_c) is facilitated by the utilization of emission spectra [37]. In this study, the emission colour of Dy^{3+} ion-incorporated ZnP glasses was ascertained using emission spectra under a stimulation wavelength of 350 nm. To express the emission colour, colour coordinates (x_c, y_c) were established. The CIE chromaticity chart of the prepared ZnP glasses containing Dy^{3+} ions is depicted in Fig. 12. From the obtained colour coordinates (x_c, y_c), correlated colour temperature (CCT) values are evaluated using the McCamy formula [19, 64]. Correlated colour temperature (CCT) values are

Table 12 CIE 1931 chromaticity colour coordinates (x_c, y_c), correlated colour temperatures (CCT, K) and yellow to blue luminescence ratio (Y/B) values of Dy^{3+} ions incorporated glasses

Glass System	Chromaticity Coordinates		CCT	Y/B Ratio
	x_c	y_c	Kelvin K	
ZnP01Dy [Present work]	0.318	0.348	6140	1.11
ZnP05Dy [Present work]	0.323	0.349	5917	1.13
ZnP10Dy [Present work]	0.325	0.356	5810	1.15
ZnP15Dy [Present work]	0.325	0.360	5787	1.17
ZnP20Dy [Present work]	0.328	0.365	5676	1.20
DFBP (Phosphate) [60]	0.383	0.419	4203	1.44
DP3(Phosphate) [19]	0.350	0.390	4955	1.59
BSLNAD5 (Boro silicate) [61]	0.340	0.360	5095	1.98
OFLZBSD0.1(Silicate) [53]	0.377	0.408	4548	1.84
Dy05 (Borate) [62]	0.3662	0.4066	4558	1.45
NBZD05 (Borate) [63]	0.38	0.42	4264	1.54
PPbTBDy1.0 (Tellurite) [13]	0.367	0.423	4586	-
PCBTD1(Fluorophosphate) [54]	0.40	0.45	4005	-
GTS: Dy (Tellurite) [64]	0.43	0.46	3510	-
NaBiSrP0.1(Phosphate) [36]	0.382	0.419	4194	-
DBS10 (Silicate) [66]	0.350	0.390	4846	-
OFSZBSDy1.0 (Silicate) [67]	0.370	0.410	4413	-
PCKZ: D2 [68]	0.389	0.434	4246	-
KZDy (Phosphate) [48]	0.425	0.456	3565	-
SBTZBD5 (Borate) [23]	0.444	0.473	3363	-
Standard white light illuminates D65 [13]	0.310	0.340	6504	-
Standard white light illuminates D50 [32]	0.333	0.333	5455	-

typically employed to measure colour sensitivity and brightness [65]. A higher CCT value signifies increased brightness and colour perception [24]. These values allow us to classify white light into three regions: (i) warm-white light, which is between 2700 and 4000 K; (ii) bright white light, which is between 4000 and 5000 K; and (iii) cool white light, which is above 5000 K [32]. The obtained colour coordinates (x, y) and CCT values are presented in Table 11. The colour coordinates of prepared ZnP glasses are in close proximity to the standard white light illuminates D50 (0.333, 0.333) [32], and D65 (0.310, 0.340) [13]. Among the prepared ZnP glasses, the colour coordinates (0.318, 0.348) of the ZnP01Dy glass are close to the colour coordinates of the standard white light illuminate D65. On the other hand, the colour coordinates of ZnP05Dy, ZnP10Dy, ZnP15Dy, and ZnP20Dy glasses were (0.323, 0.349), (0.325, 0.356), (0.325, 0.360), and (0.328, 0.365), respectively, which are in close proximity to the standard white light illuminate D50 colour coordinates. The CCT values of the prepared ZnP glasses ranged from 5676 to 6140 K, which falls within the range of cool white light (5000–6500 K) [13]. The results also demonstrate that the CCT values of the prepared ZnP glasses are higher than those of other reported PPbTBDy1.0 [13], DP3 [19], BSLNAD5 [61], KZDy [48], OFLZBSD0.1 [53], PCBTD1 [54], GTS: Dy [64], NaBiSrP0.1 [36], DBS10 [66], OFSZBSDy1.0 [67], PCKZ: D2 [68], DFBP [60], Dy05 [62], NBZD05 [63], and SBTZBD5 [23] glass matrixes doped with Dy^{3+} ions, and ZnP01Dy's CCT value (6140 K) is close to that of standardised white light illuminate D65. The Maximum CCT value and Y/B intensity

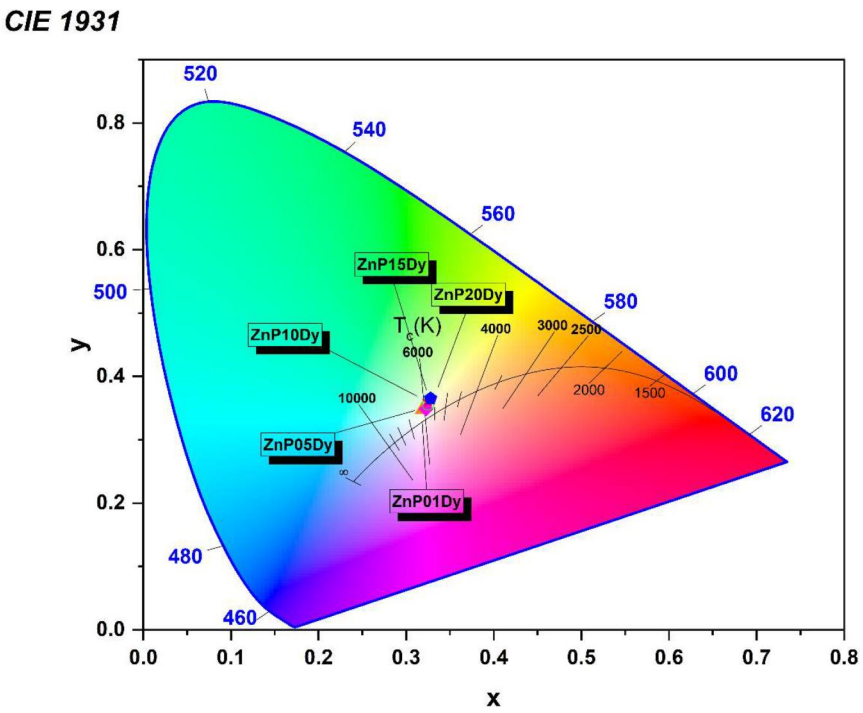

Fig. 12 CIE 1931 chromaticity colour diagram of different concentrations of Dy^{3+}ion-incorporated ZnP glasses excited at 350 nm

ratio nearly equal to unity is good selection for white light materials [69]. Therefore, the results suggests that fabricated Dy^{3+} ion-incorporated ZnP glasses are well suitable for generation of good white light [18].

Conclusion

A comprehensive study was conducted to evaluate the integration of Dy^{3+} ions into zinc phosphate glasses, aiming for white light emission in solid-state photonic devices. Several characterizations have resulted in significant findings, including the following.

- The XRD patterns and SEM-EDX mapping analyses showed that the zinc phosphate glasses had an amorphous nature and uniform elemental distribution. Fourier-transform infrared (FT-IR) and Raman spectroscopies confirmed the presence of zinc and phosphate networks.
- Judd-Ofelt theory applied to the absorption spectra and JO intensity parameters (Ω_2, Ω_4, Ω_6) were evaluated for the zinc phosphate glasses. These parameters followed the trend $\Omega_6 > \Omega_2 > \Omega_4$.
- From the absorption spectra according to the JO theory, various radiative properties were estimated.
- ZnP01Dy glass showed high total transition probabilities (A_T) of 1913 s^{-1} and short radiative lifetime (τ_{rad}) of 522 µs for $^6F_{5/2}$ level. and it displayed a higher stimulated absorption cross-section (σ_{abs}) value of 1.62×10^{-18} cm^2 for the level from $^4F_{9/2}$ to $^6H_{13/2}$.
- Primary emission colours were observed at 481 nm (blue), 572 nm (yellow), and 661 nm (red) in the luminescence spectra measured under excitation at 350 nm for the ZnP glasses doped with Dy^{3+} ions. Remarkably, the yellow band at 572 nm was more intense compared to the blue band at 481 nm.
- The emission transition $^4F_{9/2} \rightarrow {}^6H_{13/2}$ (yellow band) of the ZnP01Dy glass was found to have higher radiative transition probabilities (1027.7 s^{-1}), experimental branching ratios (51.3%), stimulated emission cross-Sect. (2.85×10^{-21} cm^2), gain bandwidths (0.05×10^{-25} cm^3).
- For the ZnP01Dy glass, the Y/B intensity ratio (1.11) was nearly equal to unity.
- Among the prepared ZnP glasses, ZnP01Dy glass was found to have colour coordinates (0.318, 0.348) which was in close proximity to the standard white light illuminate D65 (0.310, 0.340), and high CCT value of 6140 K.

The findings of this study indicate that zinc phosphate (ZnP) glasses incorporated with a concentration of 0.1 mol% Dy^{3+} ions are good candidates for generating optimal white light.

Supplementary Information The online version contains supplementary material available at https://doi.org/10.1007/s12596-024-02136-x.

Acknowledgements One of the authors, S. Vidya Sagar, thanks the government's funding agency, UGC, Govt. of India, New Delhi, for providing financial support in the form of JRF under UGC-CSIR NET-JRF (No. F. 82 – 1/2018(SA-III), and UGC-Ref. No.191620143937, issued on 05/20/2020, which enabled him to carry out this research. The authors thank Mr. Essaki Kumar, a laboratory technician at CIF Pondicherry University, who helped to obtain Raman, optical absorption, excitation, emission data; the Faculty of Physics at Yogi Vemana University for facilitating the instrumentation of XRD and SEM-EDX; and the Laboratory Technician at Lovely Professional University (LPU), Jalandhar for facilitating the instrumentation of FTIR.

Author contributions SVS: Conceptualization, Methodology, Validation, Investigation, Writing-Original draft preparation, Visualization, KVR: Conceptualization, Investigation, Writing-Review & Editing, Supervision. SB: Conceptualization, Investigation, Writing-Review & Editing, Visualization, SA: Conceptualization, Investigation, Writing-Review & Editing, Visualization.

Funding This study was supported by the government's funding agency, University Grants Commission (UGC), Government of India, New Delhi, in the form of a Junior Research Fellowship (JRF) under UGC-CSIR NET-JRF, No.F.82 – 1/2018(SA-III), UGC-Ref. No.: 191620143937, issued on 05/20/2020 to S. Vidya Sagar.

Data availability Data will be made available on reasonable request.

Declarations

Competing Interests The authors declared that they have no relevant financial or non-financial interests to disclose.

References

1. A. Vidhi, Anu, A.S. Rao, Opt. Mater. (Amst). **132**, 112863 (2022). https://doi.org/10.1016/j.optmat.2022.112863
2. S.A. Ansari, M.O. Ansari, A. Alshahrie, M. Shahadat, N. Parveen, R. Darwesh, S.F. Aboushoushah, Appl. Sci. (Switzerland). **12**(5), 2632 (2022). https://doi.org/10.3390/app12052632
3. E. Cantelar, G. Lifante, L. Grima, J.I. Peña, D. Sola, J. Lumin. **253**, 119484 (2023). https://doi.org/10.1016/j.jlumin.2022.119484
4. T.N.L. Tran, A. Szczurek, A. Lukowiak, A. Chiasera, Opt. Materials: X. **13**, 100140 (2022). https://doi.org/10.1016/j.omx.2022.100140
5. X. Chen, A.V. Khamenok, S.G. Khusainov, M.V. Shestakov, V.V. Moshchalkov, Optics. **4**, 66 (2023). https://doi.org/10.3390/opt4010006
6. C.S. Sarumaha, N. Wantana, J. Rajagukguk, J. Kaewkhao, *J Phys Conf Ser* (IOP Publishing Ltd), (2021) https://doi.org/10.1088/1742-6596/2013/1/012020
7. M. Emara, E.S. Yousef, J. Mod. Opt. **65**, 1839 (2018). https://doi.org/10.1080/09500340.2018.1461942
8. D. He, Y. Fang, M. Liao, G. Zhao, Y. Sun, F. Yu, L. Hu, X. Wang, J. Hou, T. Xue, Y. Liu, J. Lumin. **236**, 118087 (2021). https://doi.org/10.1016/j.jlumin.2021.118087
9. T.S. Dhapodkar, A.R. Kadam, N. Brahme, S.J. Dhoble, Mater. Today Chem. **24**, 100938 (2022). https://doi.org/10.1016/j.mtchem.2022.100938

10. M. Dhavamurthy, P. Vinothkumar, M. Mohapatra, A. Suresh, P. Murugasen, Spectrochim Acta Mol. Biomol. Spectrosc. **266**, 120448 (2022). https://doi.org/10.1016/j.saa.2021.120448
11. F. Khrongchaiyaphum, N. Wantana, C.S. Sarumaha, E. Kaewnuam, S. Kothan, N. Chanthima, J. Kaewkhao, Radiat. Phys. Chem. **201**, 110442 (2022). https://doi.org/10.1016/j.radphyschem.2022.110442
12. P.A.J. Joseph, K. Maheshvaran, I.A. Rayappan, in *AIP Conf Proc* (American Institute of Physics Inc.,), (2019) https://doi.org/10.1063/1.5098614
13. J. Biswas, S. Jana, Opt. Mater. (Amst). **141**, 113932 (2023). https://doi.org/0.1016/j.optmat.2023.113932
14. S.Y. Marzouk, H.M. Elsaghier, W. Abbas, N.A. Zidan, M.A. Azooz, Results Chem. **4**, 100395 (2022). https://doi.org/10.1016/j.rechem.2022.100395
15. S. Bairagi, K.S. Bartwal, G.F. Ansari, Mater. Today Proc. **80**, 799 (2023). https://doi.org/10.1016/j.matpr.2022.11.131
16. M. Monisha, N. Mazumder, S.K. Melanthota, B. Padasale, A.H. Almuqrin, M.I. Sayyed, N. Karunakara, S.D. Kamath, Opt. Mater. (Amst). **128**, 112447 (2022). https://doi.org/10.1016/j.optmat.2022.112447
17. V. Chandrappa, C. Basavapoornima, V. Venkatramu, S.R. Depuru, J. Kaewkhao, W. Pecharapa, C.K. Jayasankar, Optik (Stuttg). **266**, 169583 (2022). https://doi.org/10.1016/j.ijleo.2022.169583
18. R. Ruamnikhom, P. Yasaka, K. Boonin, P. Limsuwan, J. Kaewkhao, Radiat. Phys. Chem. **202**, 110485 (2023). https://doi.org/10.1016/j.radphyschem.2022.110485
19. M. Shwetha, B. Eraiah, J. Non Cryst. Solids. **555**, 120622 (2021). https://doi.org/10.1016/j.jnoncrysol.2020.120622
20. R. El-Adawy, H.A. El-Mallawany, Elabd, I.A. El-Mesady, Results Opt. **8**, 100234 (2022). https://doi.org/10.1016/j.rio.2022.100234
21. J. Dahiya, A. Hooda, A. Agarwal, S. Khasa, J. Non Cryst. Solids. **576**, 121237 (2022). https://doi.org/10.1016/j.jnoncrysol.2021.121237
22. V. Chandrappa, C. Basavapoornima, C.R. Kesavulu, A.M. Babu, S.R. Depuru, C.K. Jayasankar, J. Non Cryst. Solids. **583**, 121466 (2022). https://doi.org/10.1016/j.jnoncrysol.2022.121466
23. H.A. Thabit, A.K. Ismail, G. Jagannath, A.I.S. Hashim, M.I. Sayyed, J. Non Cryst. Solids. **608**, 122258 (2023). https://doi.org/10.1016/j.jnoncrysol.2023.122258
24. V. Anthony Raj, A. Josuva, K. D'Silva, M.M. Maheshvaran, Armstrong Arasu, I Rayappan Phys. B Condens. Matter. **651**, 414590 (2023). https://doi.org/10.1016/j.physb.2022.414590
25. Kashif, A. Ratep, Results Opt. **11**, 100401 (2023). https://doi.org/10.1016/j.rio.2023.100401
26. M. Kuwik, A. Górny, W.A. Pisarski, J. Pisarska, Spectrochim Acta Mol. Biomol. Spectrosc. **268**, 120693 (2022). https://doi.org/10.1016/j.saa.2021.120693
27. S. Abdullahi, M.I. Hashim, Sayyed, S.K. Ghoshal, Heliyon. **9**(5) (2023). https://doi.org/10.1016/j.heliyon.2023.e15906. e15906
28. Kashif, A. Ratep, Boletin De La Sociedad Espanola De Ceramica Y Vidrio 61, 622 (2022). https://doi.org/10.1016/j.bsecv.2021.06.001
29. M.K. Komal Poojha, M. Vijayakumar, P. Matheswaran, E. Sayed, Yousef, K. Marimuthu, Opt. Laser Technol. **156** (2022). https://doi.org/10.1016/j.optlastec.2022.108585
30. V.R.L. Murty, M. Venkateswarlu, K. Swapna, S. Mahamuda, P. Rekha, Rani, A.S. Rao, Polyhedron. **227**, 116137 (2022). https://doi.org/10.1016/j.poly.2022.116137
31. P. Ramakrishna, S. Panda, P. Vinodkumar, R.K. Padhi, H. Jena, B.S. Panigrahi, J. Non Cryst. Solids. **566**, 120883 (2021). https://doi.org/10.1016/j.jnoncrysol.2021.120883
32. M. Monisha, N. Mazumder, G. Lakshminarayana, S. Mandal, S.D. Kamath, Ceram. Int. **47**(1), 598 (2021). https://doi.org/10.1016/j.ceramint.2020.08.167
33. P. Manyum, W. Rittisut, P. Mool-am-kha, C. Ekwongsa, N. Wantana, Y. Ruangtaweep, M. Popanao, S. Rujirawat, R. Yimnirun, P. Kidkhunthod, A. Prasatkhetragarn, S. Kothan, H.J. Kim, J. Kaewkhao, Radiat. Phys. Chem. **206**, 110801 (2023). https://doi.org/10.1016/j.radphyschem.2023.110801
34. O. Kıbrıslı, A.E. Ersundu, M.Ç. Ersundu, J. Non Cryst. Solids. **513**, 125 (2019). https://doi.org/10.1016/j.jnoncrysol.2019.03.020
35. H. Liang, X. Liu, J. Tong, P. He, Z. Zhou, Z. Luo, A. Lu, Ceram. Int. **49**, 15266 (2023). https://doi.org/10.1016/j.ceramint.2023.01.110
36. H. George, N. Deopa, S. Kaur, A. Prasad, M. Sreenivasulu, M. Jayasimhadri, A.S. Rao, J. Lumin. **215**, 116693 (2019). https://doi.org/10.1016/j.jlumin.2019.116693
37. M. Kumar, R.P. Vijayalakshmi, Y.C. Ratnakaram, J. Mol. Struct. **1265**, 133333 (2022). https://doi.org/10.1016/j.molstruc.2022.133333
38. H. Liang, Z. Luo, K. Wu, J. Tong, Z. Zhou, A. Lu, Opt. Mater. (Amst). **135**, 113256 (2023). https://doi.org/10.1016/j.optmat.2022.113256
39. V.B. Sreedhar, N. Vijaya, D. Ramachari, C.K. Jayasankar, J. Mol. Struct. **1130**, 1001 (2017). https://doi.org/10.1016/j.molstruc.2016.10.062
40. W.T. Carnall, P.R. Fields, K. Rajnak, J. Chem. Phys. **49**(10), 4424 (1968). https://doi.org/10.1063/1.1669893
41. Mariselvam, J. Liu, Opt. Mater. (Amst). **114**, 110997 (2021). https://doi.org/10.1016/j.optmat.2021.110997
42. D. Siva Raju, B. Deva Prasad Raju, S. Hima Bindu, M. Hema Latha, J. Suresh Krishna, V.V. Krishna, and C. Linga Raju, *Mater Today Proc* (Elsevier Ltd, 2021), 4364–4372. https://doi.org/10.1016/j.matpr.2021.05.087
43. Maheshwari, A.S. Rao, Opt. Mater. (Amst). **129**, 112518 (2022). https://doi.org/10.1016/j.optmat.2022.112518
44. Mariselvam, J. Liu, Opt. Laser Technol. **140**, 106944 (2021). https://doi.org/10.1016/j.optlastec.2021.106944
45. T. Jose, J.R. Krishnapriya, C. Jose, Joseph, P.R. Biju, Phys. B Condens. Matter. **634**, 413772 (2022). https://doi.org/10.1016/j.physb.2022.413772
46. S.N. Fadhilah Zalamin, M.H. Mohd Zaid, K.A. Matori, M.K. Abdul Karim, N.A. Mohamad, Yamin, N.A. Nazihah, Ismail, J. Phys. Chem. Solids. **163** (2022). https://doi.org/10.1016/j.jpcs.2021.110563
47. M. Bhemarajam, Swapna, P. Mohan Babu, Syam Prasad, M. Prasad, Opt. Mater. (Amst). **113**, 110818 (2021). https://doi.org/10.1016/j.optmat.2021.110818
48. E.F. Huerta, O. Soriano-Romero, A.N. Meza-Rocha, U. Caldiño, J. Lumin. **257**, 119617 (2023). https://doi.org/10.1016/j.jlumin.2022.119617
49. W.A. Pisarski, Materials. **15**(24), 9042 (2022). https://doi.org/10.3390/ma15249042
50. B. Klimesz, W. Ryba-Romanowski, R. Lisiecki, Opt. Mater. (Amst). **42**, 538 (2015). https://doi.org/10.1016/j.optmat.2015.02.012
51. G.F. Wetenkamp, West, H. Többen, J. Non Cryst. Solids. **140**, 35 (1992). https://doi.org/10.1016/S0022-3093(05)80737-9
52. R. Lisiecki, J. Komar, B. Macalik, M. Glowacki, M. Berkowski, W. Ryba-Romanowski, Materials. **14**(9), 2370 (2021). https://doi.org/10.3390/ma14092370
53. S. Poonam, A. Anu, M.K. Kumar, P.R. Sahu, N. Rani, R. Deopa, Punia, A.S. Rao, J. Non Cryst. Solids. **544**, 120187 (2020). https://doi.org/10.1016/j.jnoncrysol.2020.120187
54. R. Divina, P.E. Teresa, K. Marimuthu, J. Alloys Compd. **883**, 160845 (2021). https://doi.org/10.1016/j.jallcom.2021.160845
55. P. Babu, V. Chandrappa, N. Vijaya, C.K. Jayasankar, H.J. Seo, Phys. B Condens. Matter. **614**, 413037 (2021). https://doi.org/10.1016/j.physb.2021.413037
56. Jha, M. Jayasimhadri, J. Alloys Compd. **688**, 833 (2016). https://doi.org/10.1016/j.jallcom.2016.07.024

57. N.B.D.S.R.P.V.V.L. Vijaya, Y.C. Ratnakaram, Optik (Stuttg). **192**, 162980 (2019). https://doi.org/10.1016/j.ijleo.2019.162980
58. N. Kiwsakunkran, H.J. Chanthima, P. Kim, Kidkhunthod, J. Kaewkhao, Radiat. Phys. Chem. **208**, 110890 (2023). https://doi.org/10.1016/j.radphyschem.2023.110890
59. M. Rekha Rani, S. Venkateswarlu, K. Mahamuda, N. Swapna, Deopa, A.S. Rao, J. Alloys Compd. **787**, 503 (2019). https://doi.org/10.1016/j.jallcom.2019.02.088
60. M. Murugasen, P. Dhavamurthy, A. Anthoniammal, Antony Suresh, M. Mohapatra, Spectrochim Acta Mol. Biomol. Spectrosc. **308**, 123757 (2024). https://doi.org/10.1016/j.saa.2023.123757
61. S. Elkhoshkhany, M. Marzouk, H. El–Sherbiny, M.S. Anwer, H. Alqahtani, M. Algarni, Reben, E. Sayed Yousef, Results Phys. **27**, 104544 (2021). https://doi.org/10.1016/j.rinp.2021.104544
62. S. Hemalatha, M. Nagaraja, A. Madhu, N. Srinatha, Results Opt. **9**, 100275 (2022). https://doi.org/10.1016/j.rio.2022.100275
63. Roopa, B. Eraiah, J. Non Cryst. Solids. **551**, 120394 (2021). https://doi.org/10.1016/j.jnoncrysol.2020.120394
64. J.N. Lisiecki, Cryst. Solids. **597**, 121922 (2022). https://doi.org/10.1016/j.jnoncrysol.2022.121922
65. G. Lakshminarayana, A.N. Meza-Rocha, O. Soriano-Romero, U. Caldiño, A. Lira, J. Yoon, J. Non Cryst. Solids. **622**, 122660 (2023). https://doi.org/10.1016/j.jnoncrysol.2023.122660
66. T. Jose, J. Krishnapriya, A. George, C. Baby, Joseph, P.R. Biju, J. Phys. Conf. Ser. (Institute Phys. (2022). https://doi.org/10.1088/1742-6596/2357/1/012016
67. A. Anu, N. Kumar, Ravina, Deopa, A.S. Rao, J. Non Cryst. Solids. **616**, 122421 (2023). https://doi.org/10.1016/j.jnoncrysol.2023.122421
68. W. Zhu, A. Yang, Z. Hao, C. Cai, J. Wei, Y. Zhang, Ceram. Int. **50**, 3101 (2024). https://doi.org/10.1016/j.ceramint.2023.11.057
69. F. Zaman, N. Srisittipokakun, G. Rooh, S.A. Khattak, J. Kaewkhao, M. Rani, H.J. Kim, Opt. Mater. (Amst). **119**, 111308 (2021). https://doi.org/10.1016/j.optmat.2021.111308